Temperature-Induced Transformations in CoAPO-34 Molecular Sieve: A Combined In Situ X-ray Diffraction and FTIR Study

Annalisa Martucci,* Alberto Alberti, and Giuseppe Cruciani

Dipartimento di Scienze della Terra, Sezione di Mineralogia, Petrografia e Geofisica, Via Saragat 1 32, I-44100 Ferrara, Italy

Alberto Frache and Leonardo Marchese*

Dipartimento di Scienze e Tecnologie Avanzate, Università del Piemonte Orientale "A. Avogadro", C. so Borsalino 54, I-15100 Alessandria, Italy

Heloise O. Pastore

Instituto de Química, Universidade Estadual de Campinas, CP 6154, CEP 13083-970, Campinas, SP, Brazil

Received: February 14, 2005

Thermally induced processes of CoAPO-34, an aluminophosphate molecular sieve with chabasite-type structure, synthesized in the presence of morpholine as a structure-directing agent and HF as a mineralizing agent, have been studied by in situ X-ray synchrotron powder diffraction augmented with Fourier transform (FT) IR analysis. A time-resolved experiment was performed using a translating imaging plate system. At room temperature, the structure refinement by full-profile Rietveld analysis showed *P*-1 symmetry and the presence of one Al site with sixfold coordination. At around 400 °C, both fluorine and morpholine are lost, and the four-connected chabazite (CHA)-type topology is restored. Notwithstanding the metrically rhombohedral values of the cell parameters, the symmetry remains triclinic *P*-1. Inhomogeneous dealumination of the framework begins at 725 °C, accompanied by a strong triclinization of the unit cell and followed by the collapse of the structure above 775 °C. The insertion of cobalt ions within the CHA framework was monitored by FTIR spectroscopy, which showed that bridged $Co^{2+}-O(H)-P$ hydroxyls are present after morpholine removal.

Introduction

The response of zeolites and $AlPO_4$ molecular sieves on heating is not only of academic significance but also of potential industrial importance. A number of factors contribute to the macroscopically observable thermal effects such as evolution of H_2O and encapsulated organic species, variation in unit-cell volume, and structural breakdown or modification.[1,2] These effects, which modify the pore and channel geometry, affect the absorption and diffusion of molecules in zeolites and microporous $AlPO_4$ catalysts and, consequently, the catalytic properties of materials[3]. When cobalt ions are incorporated into the tetrahedral framework sites of microporous aluminophosphates ($AlPO_4$), selective heterogeneous catalysts are produced which may combine both redox and acidic properties.[4−6] CoAPO-34, for instance, a material with chabazite-related framework, is a particularly good shape-selective acid catalyst for methanol-to-olefin[7] oxidation as well as redox catalyst for NO-to-NO_2 oxidation.[8,9]

Several spectroscopic techniques, including UV−vis, electron paramagnetic resonance (EPR), and extended X-ray absorption fine structure (EXAFS), as well as X-ray diffraction, have been used[5,6,10−13] to recognize that Co^{2+} may isomorphously substitute for Al^{3+} in the framework of ALPO-*n* (*n* = 5, 11, 16, 21, 34, 36, 53). Clear-cut evidence that the negative charge of the framework is balanced by protons, thus producing Brønsted acidity, has been found by FTIR, which was used to monitor bridged $Co^{2+}-O(H)-P$ hydroxyls.[12−15] Spectroscopic studies combined with thermal analysis provided evidence of the presence of structural cobalt ions, after which the templating organic molecules, encapsulated within the molecular sieve cages during the hydrothermal synthesis, were removed by calcination. These studies demonstrated that, besides Co^{2+} Lewis acid centers, structural Co^{3+} was formed upon oxidation, and the bridged hydroxyls disappeared. Diffraction studies of dehydration processes in zeolites have been carried out by using Rietveld structure analysis of temperature-resolved powder diffraction data collected with synchrotron radiation (refs 16−19 and references therein). This is, in fact, the most well suited experimental technique for studying temperature-induced structural transformations. However, in situ variable-temperature powder diffraction, combined with Rietveld analysis, for the detailed description of the structural modifications has never been used for $AlPO_4$ molecular sieves.

The present investigation provides an exhaustive picture of the structural modifications upon removal of fluorine and thermal degradation of morpholine, used as a structural directing agent during the synthesis of CoAPO-34, by means of an in situ temperature-resolved powder diffraction study using synchrotron radiation.

* Corresponding authors. Phone +39-0532-293752, fax +39-0532-293752, e-mail mrs@dns.unife.it (A.M.). Phone +39-0131-287435, fax +39-0131-287416, e-mail leonardo.marchese@mfn.unipmn.it (L.M.).

10.1021/jp050777k CCC: $30.25
Published on Web 06/22/2005

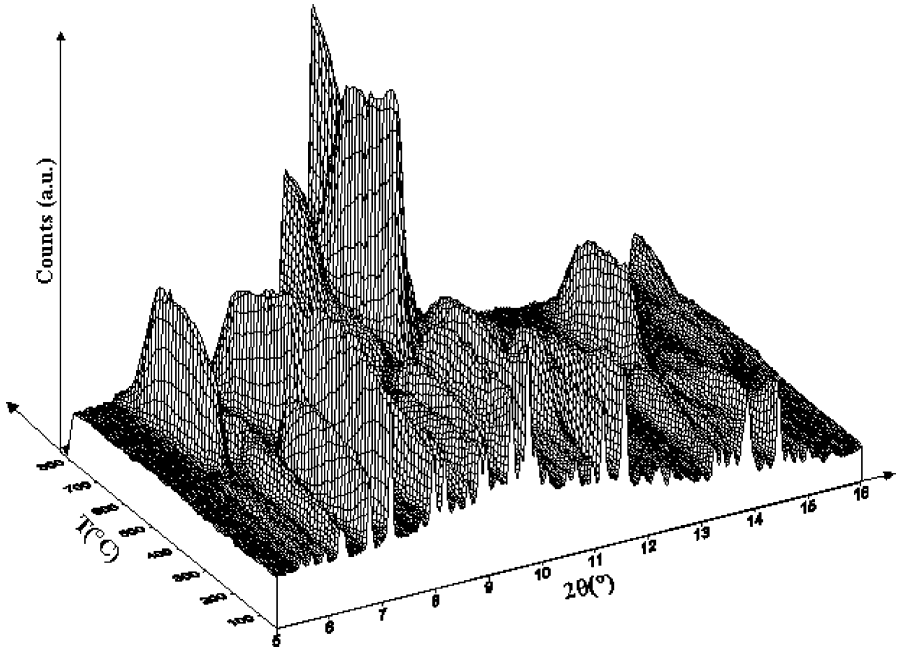

Figure 1. Evolution of the X-ray powder diffraction (XRPD) patterns in the 5−16° 2θ interval as a function of the temperature during the in situ experiment.

Experimental Section

1. Synthesis. CoAPO-34 was synthesized by mixing appropriate amounts of $Al(OH)_3$, H_3PO_4, and distilled water and stirred until a uniform gel was obtained. $Co(CH_3COO)_2$ and HF were then added, followed by morpholine. The resulting gel (0.08 Co/0.92 Al/1.0 P/0.35 HF/50 H_2O/1.25 morpholine) was crystallized in a Teflon-lined static autoclave under autogenous pressure at 195 °C for 10 days. A similar procedure was also used to synthesize AlPO-34 material.[20] Small rhombohedral bluish crystals of CoAPO-34 with average size of around 5 μm were obtained.

2. Materials Characterization. A preliminary XRD characterization was performed using a Shimadzu XRD6000 with CuKα, at 2° 2θ min^{-1}, with slits of 1°, 1° and 0.3 mm for scattering, divergence, and receiving. High-temperature experiments were conducted with the aid of a Shimadzu heating accessory model HA1001, at a heating rate of 5 °C/min, from room temperature to 1000 °C.

High-resolution powder patterns of as-synthesized CoAPO-34 sample were measured at the Swiss-Norwegian Beam Line (SNBL, ESRF, Grenoble) on a triple-axis diffractometer equipped with an Si(111) analyzer crystal (wavelength of 0.953 370 Å). The sample was loaded into a glass capillary which was axially spun during data collection in the Debye−Scherrer geometry. Time-resolved diffraction data were collected at the GILDA beamline at ESRF (Grenoble), using a fixed wavelength of 0.68765 Å. The powder sample was packed into a 0.3-mm-diameter Lindemann capillary, opened at both ends, and heated in situ to 800 °C using a hot air stream; the heating rate was 5 °C/min. During the heating process, powder diffraction patterns were recorded on the 4-mm slit-delimited portion of a translating flat image plate[21] (Figure 1), which had a translation rate of 2.5 pixel/K with respect to the temperature increase. External standard LaB_6 was used to calibrate the wavelength, as well as to determine the zero-shift position, sample-to-detector distance, and tilting angle of the image plate detector.

FTIR spectra of pelletized samples were recorded at room temperature with a Bruker IFS88 spectrometer in specially designed cells permanently connected to a vacuum line. The as-synthesized materials were calcined with the following procedure: (a) heating in vacuo with a slow increase of temperature (2−3 °C/min) up to 150 °C; (b) admitting 80−100 Torr of O_2 and raising the temperature (10 °C/min) from 150 to 550 °C; (c) calcining 3−4 h at 550 °C and changing the oxygen three times; (d) evacuating at 550 °C for 20 min (final pressure $< 10^{-5}$ Torr). Prior to spectroscopic measurements, the CoAPO-34 sample was reduced in hydrogen at 350 °C for 4 h, a treatment which leads to the formation of Co^{2+}−O(H)−P bridged hydroxyls.[12,14,15] Subsequently, the sample was calcined again at 560 °C in pure oxygen, followed by a treatment under deuterium at 350 °C to obtain a deuterium-exchanged CoAPO-34 sample.

Thermogravimetric analyzer (TGA) analyses were carried out on a TA instrument (SDT2960 model) by keeping 10−15 mg of as-synthesized samples under a constant flux of air and using a heating rate of 5 °C/min. The weight loss from 25 to 700 °C was 24.4%. Chemical analysis was performed on an inductively coupled plasma mass spectrometer (ICP-MS) VG Plasma Quad 2 plus. The sample was dissolved in a mixture of HF and HNO_3. A concentration of 2.4 wt % of cobalt was found, and this corresponds to 7% of Co in the Al sites, a value close to the Co/Al ratio in the starting gel.

3. Structure Refinement. A preliminary analysis of the powder pattern obtained by the high-resolution data collected at the SNBL beamline clearly showed *P*-1 symmetry of the CoAPO-34 material and gave unit-cell parameters which strongly resembled those found by Harding and Kariuki[22] and by Simmen[23] for an AlPO-34 material. This assumption was confirmed by the structure refinement (by full-profile Rietveld analysis) performed in the *P*-1 space group using the GSAS package,[19] starting from the atomic positions found by Harding and Kariuki.[22] This structural model was used to carry out an analysis of the time-resolved data collected at the GILDA beamline at ESRF. In all refinements, the Bragg peak profile was modeled using a pseudo-Voigt function with a 0.01% cutoff of the peak intensity. The background curve was fitted using a Chebyschev polynomial with 20 variable coefficients. The 2θ− zero shift was accurately refined in all the patterns of the data

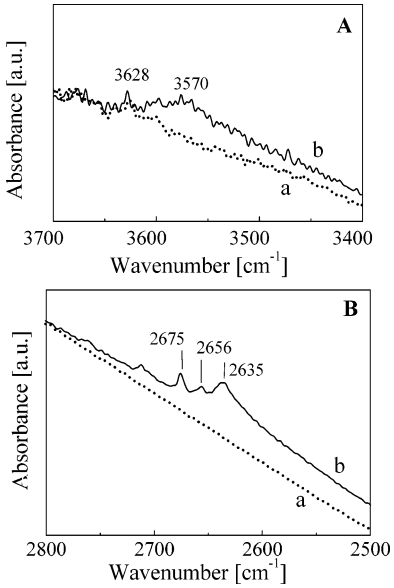

Figure 2. FTIR spectra of CoAPO-34 after calcination at 560 °C under oxygen (curves *a* in both panels) and after reduction in hydrogen at 350 °C (curve *b* in panel A) and deuterium at 350 °C (curve *b* in panel B).

set. One scale factor and the unit-cell parameters were allowed to vary for all histograms. In the final cycles, the refined structural parameters for each data histogram were the following: fractional coordinates for all atoms, occupancy factors for extraframework cations, and isotropic displacement factors (one each for tetrahedral sites, framework O atoms, morpholine O, C, and N atoms). Occupancy factors and isotropic displacement factor coefficients were varied in alternate cycles. Soft constraints were imposed on T−O distances, and the same weight was used throughout the refinement procedure. Reasonable values were obtained for C−C, C−O, and C−N bond distances, left free in all the stages of refinement.

Results and Discussion

Preliminary high-temperature X-ray diffraction (XRD) experiments were performed on CoAPO-34 and AlPO-34 samples. As far as the thermal stability of the materials is concerned, the CoAPO-34 sample keeps a chabazite-type phase up to 700 °C. This behavior is relevant for the application of CoAPO-34 as catalyst in high-temperature reactions or processes that require catalyst regeneration at high temperatures. In the case of ALPO-34, the chabazite phase is essentially retained up to 1000 °C, indicating that this material is much more stable than the Co-substituted one. Clear-cut evidence of the presence of tetrahedral cobalt ions in the aluminum position arise from FTIR measurements. Figure 2A shows the OH stretching region for a CoAPO-34 after removal of the morpholine by calcination (curve a) and after subsequent reduction under H_2 at 350 °C (curve b). It is clear that after reduction there is a formation of a new absorption at 3570 cm^{-1} corresponding to bridged Co^{2+}−O(H)−P hydroxyls. These groups disappear when the sample is treated under oxygen, a mechanism which has been described as a formation of tetrahedral Co^{3+} ions.[12,15] Unfortunately, the signal-to-noise ratio in the OH stretching region is quite poor for the CoAPO-34 material as a consequence of the presence of large microcrystalline crystals which drastically scatter the IR radiation. For this reason, a reduction in D_2 was performed, and much clearer signals obtained (Figure 2B, curve b). OD groups were found at 2675, 2656, and 2635 cm^{-1}. The bands at 2675 and 2635 cm^{-1} were assigned to P−OD and $[Co^{2+}-O(D)-P]_A$ species, respectively.[12] The band at 2656 cm^{-1}, which has never been detected, can be assigned to Brønsted acid groups located at cobalt site B, $[Co^{2+}-O(D)-P]_B$, which is structurally different from site A. This is in agreement with the fact that different Al^{3+} sites are present in the chabazite CoAPO-34 structure.

TABLE 1: Lattice Parameters and Refinement Details for CoAPO from High-Resolution SNBL Data at Room Temperature and for CoAPO at 25, 350, and 700 °C from In Situ Data, Respectively[a]

	SNBL	25 °C	350 °C	700 °C
space group	*P*−1	*P*−1	*P*−1	*P*−1
a (Å)	9.3344(2)	9.3461(8)	9.312(1)	9.317(7)
b (Å)	9.1881(1)	9.1926(8)	9.207(1)	9.349(6)
c (Å)	9.1547(2)	9.1620(9)	9.143(2)	9.263(6)
V (Å)^3	764.44(1)	766.63(1)	767.22(4)	800.18(8)
∠α (°)	88.456(2)	88.403(8)	88.39(2)	94.00(8)
∠*β* (°)	102.657(2)	102.551(8)	101.31(2)	93.96(8)
∠*γ* (°)	93.672(2)	93.736(8)	93.26(1)	94.56(6)
refined pattern 2*θ* range (°)	1.53−49	0.97−40	0.5−40.78	0.5−36.73
R_{wp} (%)	8.22	4.86	14.94	14.44
R_p (%)	5.78	3.81	9.72	9.31
R_F^2 (%)	7.11	8.7	10.30	7.23
no. of contributing reflections	2576	1812	1677	1677
N_{obs}	8911	3629	3542	3542
N_{var}	90	90	90	72

[a] Notes: high-resolution SNBL synchrotron radiation, $\lambda = 0.953370(1)$ Å and in situ data synchrotron radiation, $\lambda = 0.68765$ Å. $R_p = \sum[Y_{io} - Y_{ic}]/\sum Y_{io}$; $R_{wp} = [\sum w_i(Y_{io} - Y_{ic})^2/\sum w_i Y_{io}^2]^{0.5}$; $R_F^2 = \sum|F_o^2 - F_c^2|/\sum|F_o^2|$. Estimated standard deviations in parentheses refer to the last digit.

1. Structure Refinement at Room Temperature by High-Resolution X-ray Data. The final observed and calculated powder pattern for CoAPO-34 at room temperature (from high-resolution data) is shown in Figure 3a. Lattice parameters and refinement details are reported in Table 1; atomic coordinates, occupancy, and temperature factors are reported in Table 2; bond distances are in Table 3S in the Supporting Information.

As pointed out in the previous section, the results of our refinement strongly resemble those of AlPO-34 performed by Harding and Kariuki[22] and Simmen.[23] The symmetry is triclinic with space group *P*-1. The asymmetric unit of the framework is composed of three tetrahedral P atoms, two tetrahedrally coordinated Al atoms, and one octahedrally coordinated Al atom (Figure 4). The latter framework site is coordinated to four O and two F atoms. Therefore, the sixfold coordination of Al found in the AlPO-34 structure[22,23] is also maintained when cobalt is located in the framework (see spectroscopic results). We observed that fluorine bridged two Al atoms, whose interatomic distances were shorter than those between the other framework cations. The presence of bridging fluorine led to a distortion of the trigonal symmetry of the CHA framework. Two fully occupied sites of morpholine were found at the intersection of the six- and eight-membered rings (Figure 5). The N atoms of the morpholine molecules are suitably located for hydrogen bonding (2.63 Å) with one framework oxygen (Table 3S). Apart from the morpholine sites, the Fourier and the difference Fourier maps showed only weak and diffuse maxima. On the basis of the weight loss, a very low water content was present in the cages of CoAPO-34, spread over a number of weakly occupied sites: for this reason, we preferred to neglect their contribution to the structure refinement.

TABLE 2: Atomic Coordinates and Thermal Parameters of Framework Atoms for CoAPO from High-Resolution SNBL Data at Room Temperature and for CoAPO at 25, 350, and 700 °C from In Situ Data, Respectively[a]

		SNBL	25 °C	350 °C	700 °C			SNBL	25 °C	350 °C	700 °C
Al1	*x/a*	0.912(1)	0.909(1)	0.923(5)	0.892(14)	O7	*x/a*	0.938(2)	0.932(2)	0.954(6)	0.951(28)
	y/b	0.059(1)	0.059(2)	0.046(4)	0.012(14)		*y/b*	0.285(2)	0.280(2)	0.277(6)	0.227(22)
	z/c	0.363(1)	0.365(1)	0.379(5)	0.335(15)		*z/c*	0.728(2)	0.721(2)	0.711(5)	0.780(19)
	Uiso	0.011(4)	0.019(2)[b]	0.031(2)[b]	0.04(4)[b]		Uiso	0.007(5)	0.026(3)[b]	0.036(6)[b]	0.06(6)[b]
	frac.	1.0	1.0	1.0	1.0		frac.	1.0	1.0	1.0	1.0
Al2	*x/a*	0.082(1)	0.076(1)	0.083(3)	0.065(11)	O8	*x/a*	0.520(1)	0.526(2)	0.516(4)	0.501(14)
	y/b	0.340(1)	0.338(1)	0.347(4)	0.376(10)		*y/b*	0.833(2)	0.830(2)	0.855(7)	0.771(24)
	z/c	0.871(1)	0.867(1)	0.858(3)	0.892(13)		*z/c*	0.139(2)	0.139(3)	0.091(7)	0.073(28)
	Uiso	0.009(4)	0.019(2)[b]	0.031(2)[b]	0.04(4)[b]		Uiso	0.009(5)	0.026(3)[c]	0.036(6)[c]	0.06(6)[c]
	frac.	1.0	1.0	1.0	1.0		frac.	1.0	1.0	1.0	1.0
Al3	*x/a*	0.340(1)	0.344(1)	0.334(3)	0.341(14)	O9	*x/a*	0.808(2)	0.795(2)	0.808(5)	0.811(27)
	y/b	0.880(1)	0.880(1)	0.876(4)	0.866(13)		*y/b*	0.138(2)	0.149(2)	0.143(7)	0.054(27)
	z/c	0.108(1)	0.105(1)	0.090(6)	0.101(11)		*z/c*	0.494(1)	0.478(2)	0.489(5)	0.504(11)
	Uiso	0.017(4)	0.019(2)[b]	0.031(2)[b]	0.04(4)[b]		Uiso	0.032(5)	0.026(3)[c]	0.036(6)[c]	0.06(6)[c]
	frac.	1.0	1.0	1.0	1.0		frac.	1.0	1.0	1.0	1.0
P1	*x/a*	0.899(1)	0.902(1)	0.893(4)	0.869(13)	O10	*x/a*	0.118(2)	0.127(2)	0.114(6)	0.090(14)
	y/b	0.313(1)	0.315(2)	0.305(4)	0.311(11)		*y/b*	0.526(1)	0.525(1)	0.533(4)	0.523(15)
	z/c	0.116(1)	0.113(1)	0.113(4)	0.158(12)		*z/c*	0.855(2)	0.873(3)	0.857(8)	0.772(14)
	Uiso	0.017(4)	0.019(2)[b]	0.031(2)[b]	0.04(4)[b]		Uiso	0.091(5)	0.026(3)[c]	0.036(6)[c]	0.06(6)[c]
	frac.	1.0	1.0	1.0	1.0		frac.	1.0	1.0	1.0	1.0
P2	*x/a*	0.324(1)	0.319(2)	0.319(4)	0.329(15)	O11	*x/a*	0.271(1)	0.271(2)	0.264(6)	0.210(22)
	y/b	0.118(1)	0.118(1)	0.111(3)	0.159(11)		*y/b*	0.004(1)	−0.003(2)	0.000(6)	0.122(27)
	z/c	0.872(1)	0.876(1)	0.859(4)	0.924(14)		*z/c*	0.760(2)	0.761(2)	0.736(7)	0.789(22)
	Uiso	0.015(4)	0.019(2)[b]	0.031(2)[b]	0.04(4)[b]		Uiso	0.007(5)	0.026(3)[c]	0.036(6)[c]	0.06(6)[c]
	frac.	1.0	1.0	1.0	1.0		frac.	1.0	1.0	1.0	1.0
P3	*x/a*	0.152(1)	0.154(1)	0.152(4)	0.161(15)	O12	*x/a*	0.241(1)	0.241(2)	0.261(4)	0.258(18)
	y/b	0.853(1)	0.857(1)	0.853(4)	0.866(13)		*y/b*	0.754(2)	0.746(2)	0.734(7)	0.730(22)
	z/c	0.335(1)	0.351(2)	0.340(5)	0.332(12)		*z/c*	0.984(2)	0.987(2)	0.976(7)	0.969(24)
	Uiso	0.012(4)	0.019(2)[b]	0.031(2)[b]	0.04(4)[b]		Uiso	0.007(5)	0.026(3)[c]	0.036(6)[c]	0.06(6)[c]
	frac.	1.0	1.0	1.0	1.0		frac.	1.0	1.0	1.0	1.0
F	*x/a*	0.913(1)	0.911(2)	0.905(6)		C1	*x/a*	0.553(4)	0.537(6)	0.544(8)	
	y/b	0.897(1)	0.899(2)	0.878(4)			*y/b*	0.567(3)	0.559(5)	0.660(8)	
	z/c	0.494(1)	0.499(2)	0.497(6)			*z/c*	0.769(3)	0.780(4)	0.825(9)	
	Uiso	0.012(4)	0.026(3)[c]	0.036(6)[c]			Uiso	0.012(5)	0.037(6)	0.034(1)	
	frac.	1.0	1.0	0.765(4)			frac.	1.0	1.0	1.0	
O1	*x/a*	0.703(1)	0.718(2)	0.721(5)	0.670(26)	C2	*x/a*	0.447(3)	0.440(4)	0.380(8)	
	y/b	0.127(2)	0.123(3)	0.113(6)	0.117(29)		*y/b*	0.676(4)	0.643(5)	0.706(7)	
	z/c	0.718(1)	0.728(2)	0.742(7)	0.702(22)		*z/c*	0.717(4)	0.699(5)	0.651(10)	
	Uiso	0.012(4)	0.026(3)[c]	0.036(6)[c]	0.06(6)[c]		Uiso	0.017(5)	0.037(6)[d]	0.034(1)[d]	
	frac.	1.0	1.0	1.0	1.0		frac.	1.0	1.0	1.0	
O2	*x/a*	0.668(2)	0.670(3)	0.666(6)	0.730(25)	C3	*x/a*	0.604(4)	0.597(6)	0.669(8)	
	y/b	0.947(1)	0.941(2)	0.949(5)	0.981(19)		*y/b*	0.768(3)	0.763(5)	0.788(7)	
	z/c	0.970(1)	0.964(1)	0.981(5)	0.986(19)		*z/c*	0.568(3)	0.561(5)	0.555(9)	
	Uiso	0.012(4)	0.026(3)[c]	0.036(6)[c]	0.06(6)[c]		Uiso	0.011(6)	0.037(6)[d]	0.034(1)[d]	
	frac.	1.0	1.0	1.0	1.0		frac.	1.0	1.0	1.0	
O3	*x/a*	0.762(1)	0.778(2)	0.765(5)	0.749(20)	C4	*x/a*	0.704(3)	0.718(4)	0.766(8)	
	y/b	0.744(1)	0.754(2)	0.754(5)	0.691(24)		*y/b*	0.674(3)	0.679(4)	0.664(8)	
	z/c	0.142(2)	0.171(3)	0.125(7)	0.083(14)		*z/c*	0.634(3)	0.666(5)	0.659(8)	
	Uiso	0.012(4)	0.026(3)[c]	0.036(6)[c]	0.06(6)[c]		Uiso	0.016(5)	0.037(6)[d]	0.034(1)[d]	
	frac.	1.0	1.0	1.0	1.0		frac.	1.0	1.0	1.0	
O4	*x/a*	0.024(2)	0.034(2)	0.006(7)	−0.075(13)	N	*x/a*	0.474(3)	0.517(4)	0.523(7)	
	y/b	0.298(2)	0.301(3)	0.302(6)	0.396(23)		*y/b*	0.796(3)	0.798(4)	0.815(5)	
	z/c	0.034(1)	0.042(2)	0.011(7)	0.024(15)		*z/c*	0.614(3)	0.628(4)	0.584(7)	
	Uiso	0.025(4)	0.026(3)[c]	0.036(6)[c]	0.06(6)[c]		Uiso	0.062(6)	0.037(6)[d]	0.034(1)[d]	
	frac.	1.0	1.0	1.0	1.0		frac.	1.0	0.967(1)	0.949(1)	
O5	*x/a*	0.077(2)	0.076(3)	0.063(6)	0.135(27)	O13	*x/a*	0.667(2)	0.664(3)	0.600(5)	
	y/b	0.757(1)	0.760(2)	0.792(7)	0.862(20)		*y/b*	0.559(2)	0.556(3)	0.521(5)	
	z/c	0.728(1)	0.733(2)	0.749(6)	0.803(22)		*z/c*	0.695(2)	0.685(3)	0.707(6)	
	Uiso	0.003(5)	0.026(3)[c]	0.036(6)[c]	0.06(6)[c]		Uiso	0.030(6)	0.037(6)[d]	0.034(1)[d]	
	frac.	1.0	1.0	1.0	1.0		frac.	1.0	1.0	1.0	
O6	*x/a*	0.963(1)	0.963(2)	0.960(6)	0.944(21)						
	y/b	0.039(1)	0.040(2)	0.041(6)	0.047(24)						
	z/c	0.731(1)	0.724(2)	0.737(5)	0.576(30)						
	Uiso	0.007(5)	0.026(3)[c]	0.036(6)[c]	0.06(6)[c]						
	frac.	1.0	1.0	1.0	1.0						

[a] Note: Estimated standard deviations in parentheses refer to the last digit. [b,c,d] Isotropic thermal parameters with the same superscript were constrained to be equal in each separate refinement.

2. Refinements by In Situ X-ray Data: Temperature-Dependent Variation of the Unit-Cell Parameters. The evolution of the XRPD patterns as a function of temperature is depicted in Figure 1. The most remarkable transformation is evident at about 400 °C. Final observed and calculated powder patterns for CoAPO-34 at room temperature (from high-

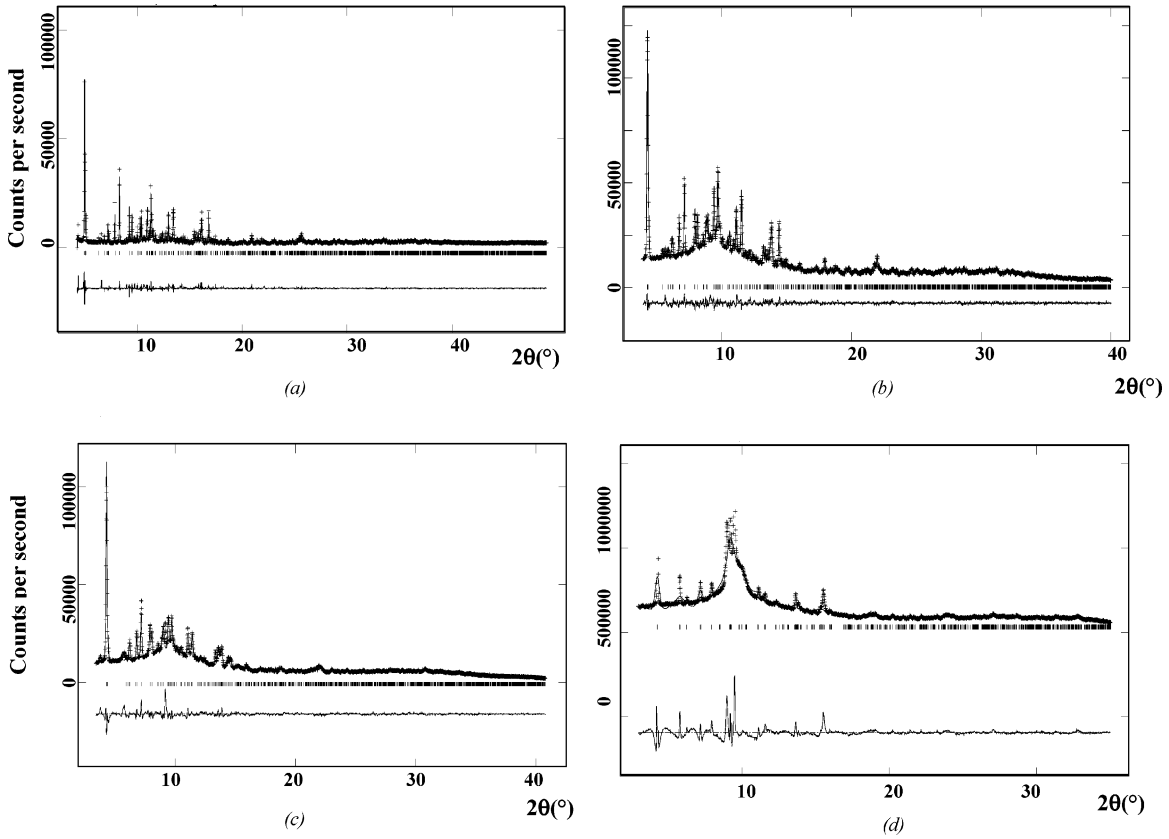

Figure 3. Observed (dotted upper line), calculated (solid upper line), and difference (solid lower line) powder diffraction patterns of CoAPO-34 at room temperature from high-resolution data (a), at 25 (b), 350 (c), 700 °C, and (d) from in situ data.

resolution data), at 350 and 700 °C (from in situ data) are shown in Figure 3b−d. Lattice parameters and refinement details are reported in Table 1.

The variations of the unit-cell parameters in the range 25−775 °C, reported in Figure 6, suggest that the temperature-induced transformations can be schematized in the following steps:

a. Temperature Range 25−375 °C. There are significant variations in the unit-cell parameters through this range; this is particularly apparent for metric parameters and angle β. These variations cause a slight increase in the cell volume starting from 150 °C (Figure 7).

b. Temperature Range 375−425 °C. A dramatic change of the unit-cell parameters occurs at about 400 °C, indicating a drastic structural rearrangement. All cell parameters take on metrically rhombohedral values, while the volume increases by around 5% (Figures 6 and 7). This transformation is to be associated with the weight loss registered by TGA at this temperature.

c. Temperature Range 425−650 °C. Cell parameters maintain their metrically rhombohedral values up to about 475 °C. Above this temperature, we observe a noticeable differentiation of metric parameters *a*, *b*, and *c*, clearly indicating a triclinic symmetry of the material studied in this work. There is also a gradual and significant reduction of the cell volume.

d. Temperature Range 650−775 °C. In this temperature range, a new process, enhanced by a strong triclinization of all unit-cell parameters and a considerable increase of the unit-cell volume, affects the structure of CoAPO-34.

3. Refinements by In Situ X-ray Data: Temperature-Dependent Structural Modifications. The results of the structure refinement show the modifications set out below:

a. Temperature Range 25−375 °C. As already discussed above, the Al1 site at 25 °C is at the center of a fairly regular octahedron, with the three angles F1−Al1−O5, F1−Al1−O11, and O6−Al1−O9 between 160° and 170°, and the other anion−Al1−anion angles in the 75−105 °C range (Figure 8). This geometry does not substantially change up to 325 °C, when some angles and distances of the polyhedron involving F start to show apparently impossible values. This behavior can be explained by examining the anion shifts and the variations in occupancy of the F site when the temperature increases (Figure 9). This occupancy is, in fact, significantly lower than 100% starting from 100 °C, and it decreases to 60% at around 325 °C without markedly modifying the geometry of the polyhedron. Above this temperature, there is a rearrangement of the polyhedron, with a consequent further loss of fluorine. The most noticeable effect is the decreasing distance between the two symmetrically dependent F sites, which reaches unacceptable values (<2 Å): these can, however, be justified by the occupancy, less than or at most equal to 50%, of the F sites, thereby permitting the alternate occupancy of F in these positions. Site Al1 thus becomes fivefold coordinated for a short temperature range; at the same time, the oxygens of the polyhedron rotate around Al1, so that the O6−Al1−O9 angle reduces to ca. 110° at 325 °C, whereas the angles around 90° in the octahedron increase to 110−120°. This fivefold coordination of Al1, however, rapidly decreases with increasing temperature, because the residual fluorine is in turn expelled, and at 425 °C, site Al1 assumes a regular tetrahedral coordination. At about 400 °C, a similar dehydrofluorination process also occurs in the fluorinated anionic aluminophosphate framework UT-6,[24] a small pore material whose structure is closely related to that of chabazite. Upon thermal treatment of UT-6, HF is

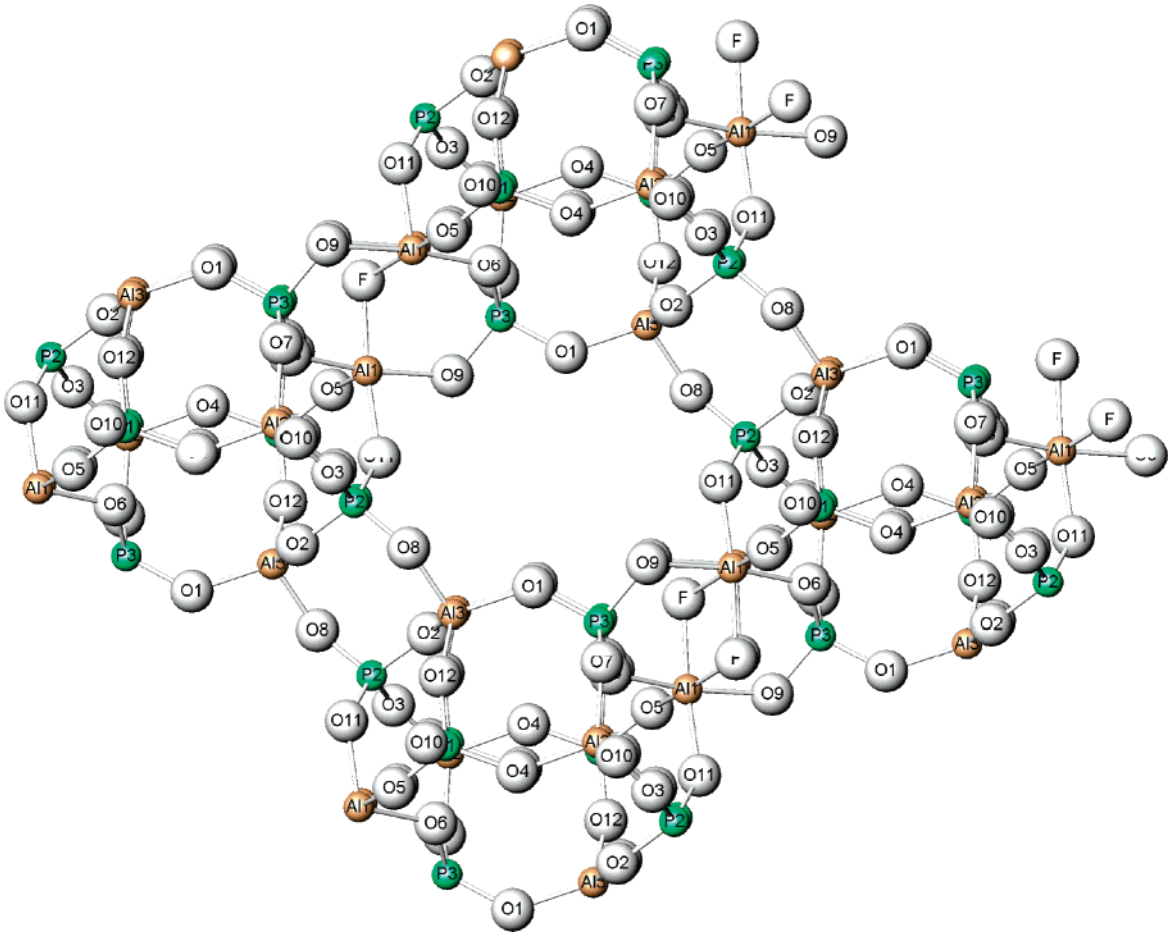

Figure 4. Projection along [010] of refined structure for CoAPO-34 at room temperature clearly showing the sixfold coordination of the Al1 atom.

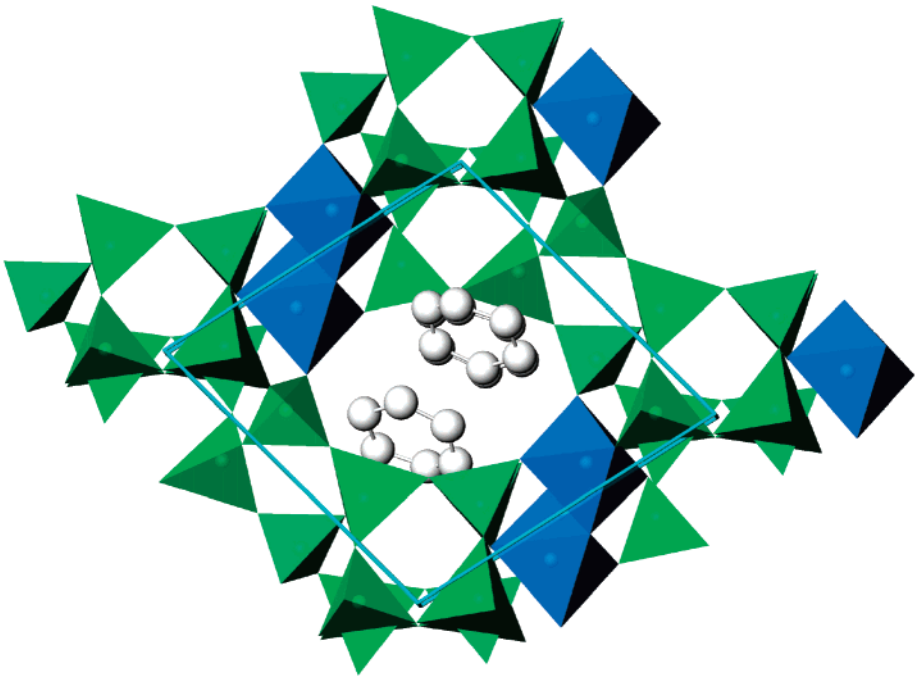

Figure 5. Projection along the [010] direction of the chabasite cage showing the organic molecules in CoAPO-34.

removed from the structure, and the material transforms into rhombohedral AlPO−CHA, as evidenced by in situ high-temperature powder X-ray diffraction, thermogravimetry, and mass spectrometry. The dehydrofluorination in CoAPO-34 and UT-6 is important, because it may render the framework useful as a solid source of hydrogen fluoride.

In this temperature range, there is also a significant variation in the shape of the eight-membered ring of the chabazite cage and in the relative T−O−T angles. At 25 °C, the ring is strongly elliptical, with the O11−O11 distance much greater than the O1−O1 (respectively, 7.30 and 5.34 Å). As the temperature rises, particularly from 100 °C, this elliptical shape tends to be

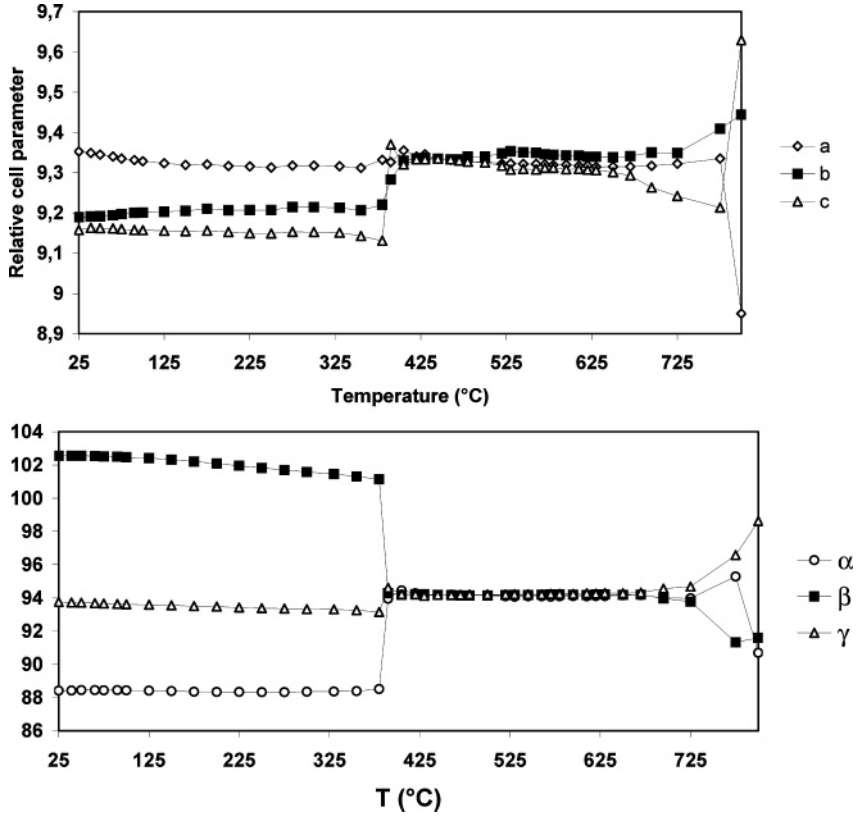

Figure 6. Temperature dependence of the unit-cell parameters of CoAPO-34. Error bars are smaller than symbols.

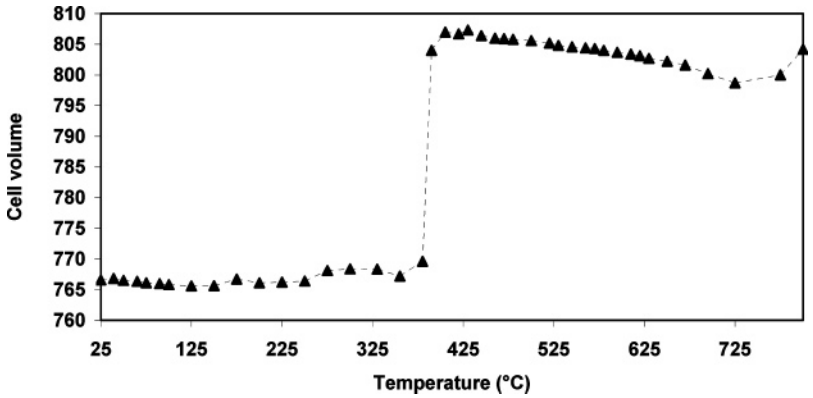

Figure 7. Plot of unit-cell volume (Å^3) vs temperature in CoAPO-34. Error bars are smaller than symbols.

lost in favor of a circular shape, although the mean of the two distances remains almost constant. This effect may be interpreted as directed at favoring the expulsion of fluorine, whose ionic radius (∼1.4 Å) requires a sufficiently wide free ring diameter. As the temperature rises, the two narrowest T−O−T angles of the eight-membered ring increase slightly (by about 15−20°), while the two largest ones remain almost unaltered, as a logical consequence of the reduced elliptical shape.

b. Temperature Range 375−425 °C. In the same range of temperature in which fluorine is lost (375−425 °C), and the three-dimensional four-connected structure of the chabazite-type phases is restored, the decomposition and expulsion of morpholine also occurs. The variation in occupancy of the organic molecule sites as a function of temperature is very fast, as can be seen in Figure 10. In fact, when morpholine begins to be expelled from the chabazite cage (about 375 °C), there is a second distortion effect of the eight-membered ring. Both the O11−O11 and O1−O1 distances suddenly increase, enlarging the free diameter of the window in order to facilitate the expulsion of fragments of decomposed morpholine and residual fluorine. As a consequence, in this temperature range, sharp increases of the T−O−T angles are recorded. The enlarging of the windows may not seem justified by the ionic radii of the atoms of morpholine: however, it cannot be excluded that fragments of morpholine are also expelled.

c. Temperature Range 425−650 °C. Following the loss of all the extraframework atoms, the eight-membered ring undergoes a third distortion effect which affects the whole temperature range: the aperture of the window progressively decreases and, the short and long axes of the eight-membered ring are inverted, so that the geometry of the ring is now analogous to that of the dehydrated H-chabazite.[25] As pointed out in the previous section, in the temperature range 425−500 °C, all cell parameters take on metrically rhombohedral values. However, the structure refinement clearly shows that the real symmetry is triclinic. The topological symmetry of the chabazite-type structure is rhombohedral *R*-3*m*, and the topochemical symmetry is rhombohedral *R*-3; as discussed above, at low temperature, the *P*-1 triclinic

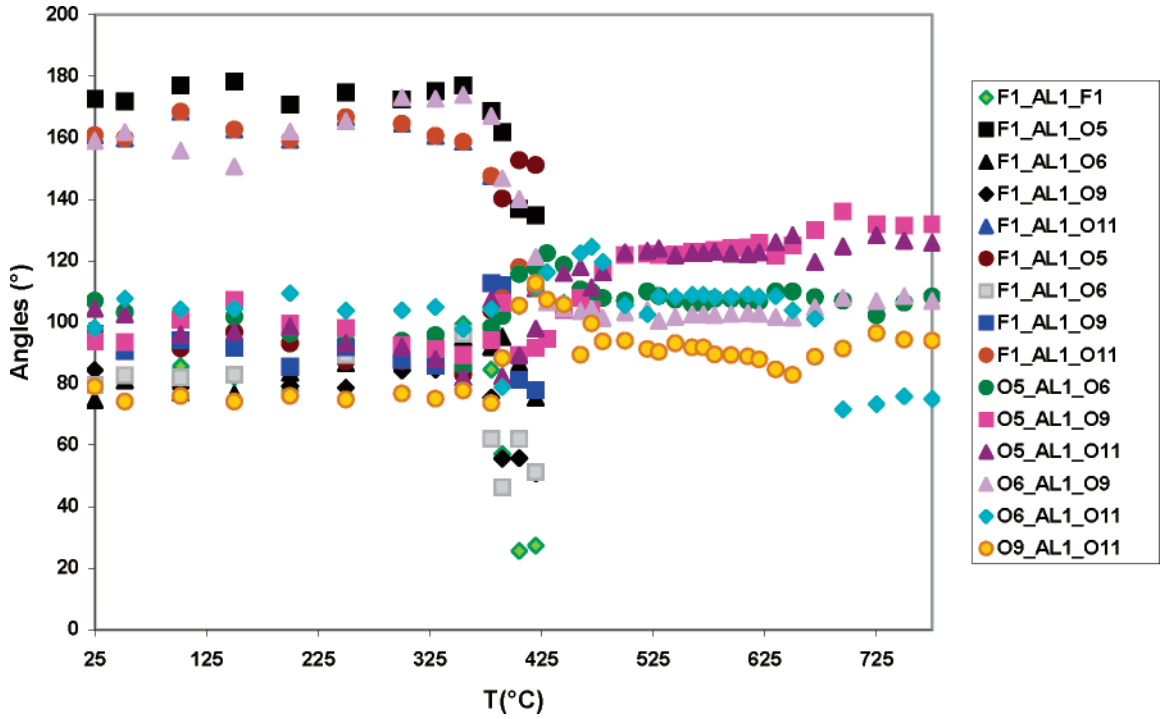

Figure 8. Variations of the geometry of the Al1 octahedron with the increase of temperature. Error bars are smaller than symbols.

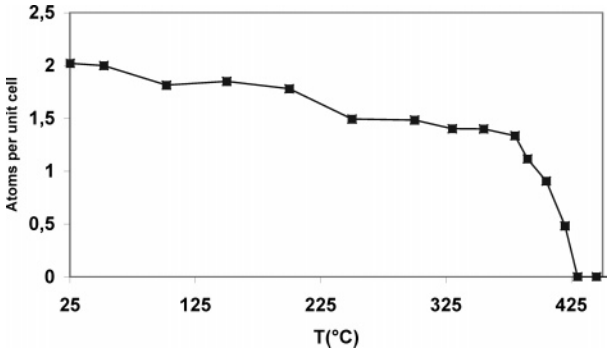

Figure 9. Variation of fluorine atoms, given as atoms per unit cell, as a function of temperature. Error bars are smaller than symbols.

symmetry is induced by the presence of two symmetrically independent Al atoms, octahedrally coordinated by fluorine atoms (Al1, see Table 3S and Figure 4) and located in the four-membered ring bridging two D6R. In this temperature range, the tetrahedral coordination of all Al atoms and the strongly pseudo-rhombohedral cell parameters could suggest that the rhombohedral symmetry is restored. Despite this, the symmetry remains triclinic *P*-1, indicating that the structure maintains a memory of the distortion imposed by the unusual coordination of Al1. This result is clearly explained by the changes in the geometry of the four-ring as a function of temperature, as shown in Figure 11. In AlPO-34-type phases with *R*-3 symmetry,[26,27] the four-rings are all symmetrically dependent, constrained by the triad; their shape is nearly square. In samples synthesized in the presence of fluorine, the three four-rings previously related by the triad are rendered symmetrically independent by the *P*-1 symmetry. Figure 11a shows that, at room temperature, the four-ring (Al1−P3−Al1−P3) bridging fluorine is strongly distorted, whereas the two others undergo only weak deformations. When fluorine is lost, the Al1−P3−Al1−P3 ring tends to be similar to the other four-rings, but not sufficiently so to restore a rhombohedral symmetry, as shown in Figure 11b (in this case,

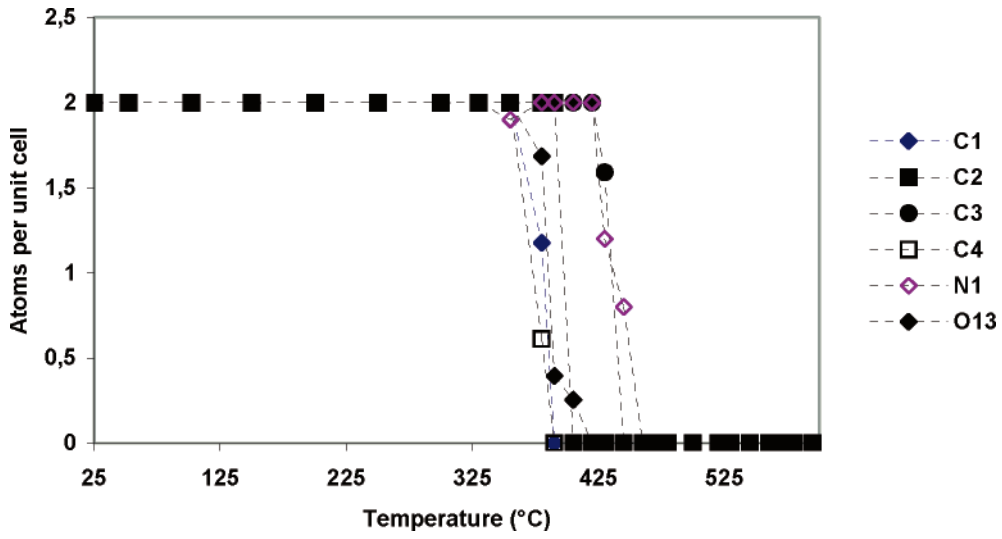

Figure 10. Variation of individual template atoms, given as atoms per unit cell, as a function of temperature. Error bars are smaller than symbols.

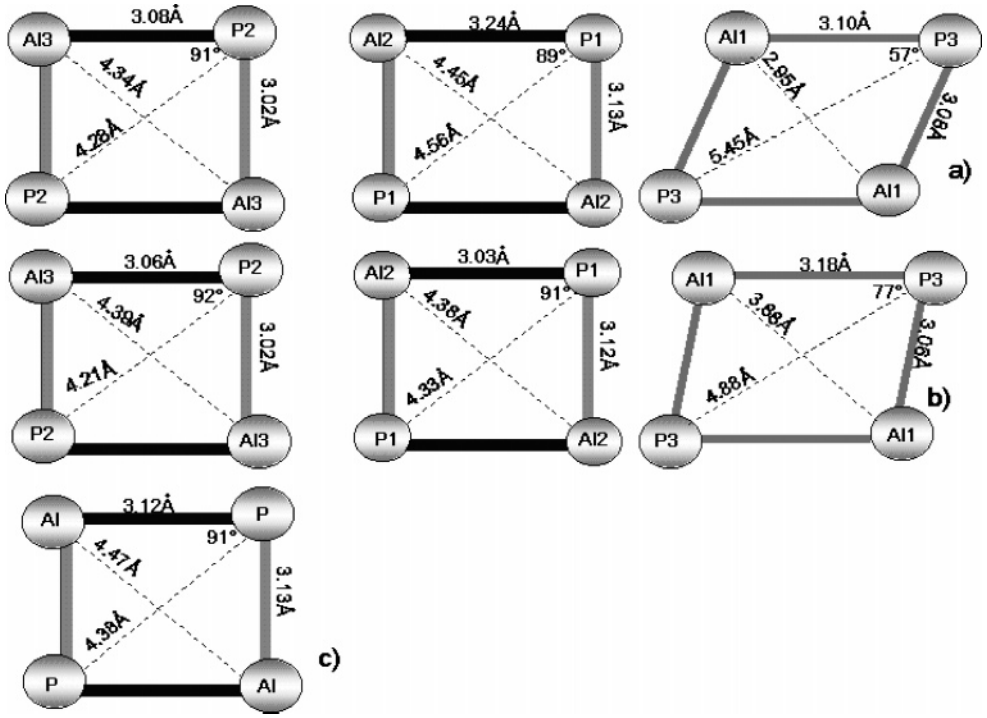

Figure 11. Geometry of the 4-ring bridging fluorine as a function of temperature.

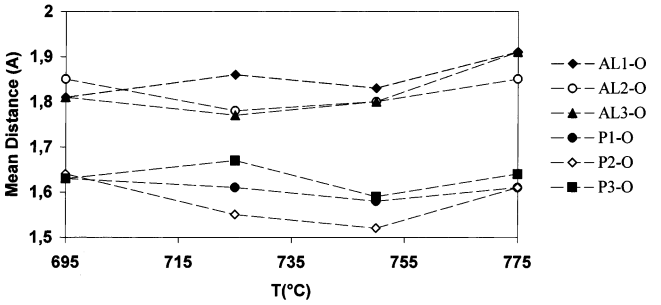

Figure 12. Variation of the tetrahedral bond distances, showing an inhomogeneous dealumination process. Error bars are smaller than symbols.

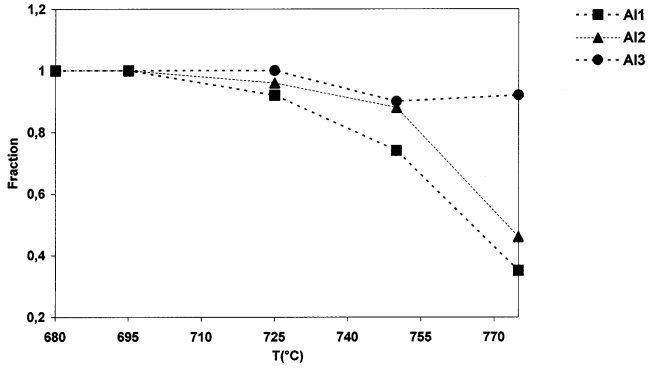

Figure 13. Variation of occupancy of aluminum atoms, showing an inhomogeneous dealumination process. Error bars are smaller than symbols.

at 500 °C). In the 525−650 °C temperature range, the triclinic symmetry is enhanced by the triclinization of the unit cell.

d. Temperature Range 650−775 °C. Above 650 °C, a new structural modification occurs which is evident from the variation of the unit-cell parameters and from the increase of the cell volume (Figures 6 and 7). As discussed above, in this temperature range, a strong triclinization of all unit-cell parameters and a considerable increase of the unit-cell volume affects the structure of CoAPO-34. The aperture of the eight-ring window progressively increases, and once more, the short and long axes of the eight-ring are inverted, so that the O11−O11 distance is now much shorter than the O1−O1. As a consequence, in this temperature range, strong variations of the T−O−T angles are recorded, and the largest concerned the eight-ring, in particular, the Al1−O11−P2, Al3−O8−P2, and Al1−O9−P3 angles. Above 775 °C, the collapse of the structure is accompanied by dealumination of the framework. The structure refinement clearly shows an increase of Al−O bond distances (Figure 12) and a simultaneous decrease of the Al site occupancies (Figure 13), clearly indicating that an inhomogeneous dealumination process occurs. Figure 13 shows that above 775 °C the dealumination process particularly involves the Al1 and Al2 sites, because their occupancies became lower than 50% of the cases. The loss of crystallinity, as evidenced by the remarkable peak broadening of patterns at temperatures, do not permit the crystal structure refinement above 775 °C.

Atomic coordinates, occupancy, and temperature factors at 25, 350, and 700 °C are reported in Table 2; bond distances are in Table 3S in the Supporting Information.

Conclusions

The in situ variable temperature XRD analysis of CoAPO-34 showed some interesting features:

a. The sixfold coordination of Al found in the AlPO-34 structures[22,23] (Al1 site) is also maintained when cobalt is located in the framework.

b. When extra-ligand species are present, they always bridge two Al atoms. This occurs independently of their nature (fluorine anions in this case or OH groups in AlPO-18,[23] AlPO-21,[28] or AlPO-14[29]) or their number (one in AlPO-18,[23] two in AlPO-21,[28] AlPO-14,[16] and AlPO-34[22,23]).

c. During the heating process, upon defluorinaxation, there is a rearrangement of the Al octahedral polyhedron, which assumes a fivefold coordination at about 400 °C. At 425 °C,

the residual fluorine is lost, and the three-dimensional four-connected chabazite-type topology is restored.

d. In the temperature range 425−475 °C, when fluorine atoms and morpholine molecules are expelled, all cell parameters take on metrically rhombohedral values. However, the real symmetry remains triclinic *P*-1, indicating that the structure maintains a memory of the distortion imposed by the unusual coordination of Al1.

e. Above 775 °C, the collapse of the structure is accompanied by an inhomogeneous dealumination of the framework which particularly concerns the Al1 and Al2 sites.

It is proposed that combined in situ XRD and FTIR studies, similar to those presented in this contribution, are of utmost relevance when structural information is needed on the modifications induced during heating treatments of molecular sieves with catalytic interst.

Acknowledgment. Italian CNR and MURST ("Catalysis for the reduction of the enviromental impact of mobile source emissions", COFIN2000, and "Zeolites, materials of interest for industry and environment: synthesis, crystal structure, stability and applications", COFIN 2001) are acknowledged for financial support. We thank the European Synchrotron Radiation Facility (ESRF) for providing beamtime. Special thanks to the SNBL (Swiss-Norwegian Beam Lines) staff for assistance during the high-resolution data collection. The authors also wish to thank Carlo Meneghini (Università di Roma Tre and OGG-INFM GILDA c/o ESRF) for support to the time-resolved powder diffraction experiments, R.E. Miller (University of Campinas) for the assistance in the high-temperature XRD experiments using conventional source and R. Tassinari (University of Ferrara) for the chemical analysis.

Supporting Information Available: Selected bond distances (Å) and angles (°) for CoAPO-34 from high-resolution SNBL data at room temperature and for CoAPO-34 at 25, 350, and 700 °C from in situ data, respectively. This material is available free of charge via the Internet at http://pubs.acs.org.

References and Notes

(1) Bish, D. L. In *Natural Zeolites '93*; Ming, D. W., Mumpton, F. A., Eds.; International Comm. Natural Zeolites: Brockport, New York, 1995; p 259.

(2) Alberti, A.; Vezzalini, G. In *Proceedings of the 6th International Zeolite Conference*; Olson, D., Bisio, A., Eds.; Butterworth: Guildford, U.K., 1983; p 834.

(3) Tschaufeser, P.; Parker, S. C. *J. Phys. Chem*. **1995**, *99*, 10609.

(4) Thomas, J. M. *Angew. Chem., Int. Ed. Engl*. **1994**, *33*, 913.

(5) Coluccia, S.; Marchese, L.; Martra, G. *Microporous. Mesoporous. Mater*. **1999**, *30*, 43.

(6) Frache, A.; Gianotti, E.; Marchese, L. *Catal. Today* **2003**, *77*, 371.

(7) Xu, Y.; Grey, C. P.; Thomas, J. M.; Cheetham, A. K. *Catal. Lett*. **1990**, *4*, 251.

(8) Frache, A.; Cadoni, M.; Coluccia, S.; Marchese, L.; Palella, B.; Pirone, R.; Ciambelli, P. *Stud. Surf. Sci. Catal*. **2001**, *135*, 328.

(9) Thomas, J. M. *Angew. Chem., Int. Ed.* **1999**, *38*, 3589.

(10) Hartmann, M.; Kevan, L. *Chem. Rev*. **1999**, *99*, 635.

(11) Baur, W. H.; Joswig, W.; Kassner, D.; Kornatowski, J. *Acta Crystallogr*. **1994**, *B50*, 290.

(12) Marchese, L.; Chen, J.; Thomas, J. M.; Coluccia, S.; Zecchina, A. *J. Phys. Chem*. **1994**, *98*, 13350.

(13) Borges, C.; Ribeiro, M. F.; Henriques, C.; Lourenço, J. P.; Murphy, D. M.; Louati, A.; Gabelica, Z. *J. Phys. Chem. B* **2004**, *108*, 8344.

(14) Marchese, L.; Gianotti, E.; Damilano, N.; Coluccia, S.; Thomas, J. M. *Catal. Lett.* **1996**, *37*, 107.

(15) Pastore, H. O.; Coluccia, S.; Marchese, L. *Annu. Rev. Mater. Res*. **2005**, *35*, 351.

(16) Martucci, A.; Sacerdoti, M.; Cruciani, G.; Dalconi, C. *Eur. J. Mineral*. **2003**, *15*, 485.

(17) Cruciani, G.; Martucci, A.; Meneghini, C. *Eur. J. Mineral*. **2003**, *15*, 257.

(18) Dalconi, M. C.; Alberti, A.; Cruciani, G. *J. Phys. Chem. B* **2003**, *107*, 12973.

(19) Milanesio, M.; Artioli, G.; Gualtieri, A.; Palin, L.; Lamberti, C. *J. Am. Chem. Soc*. **2003**, *125*, 14549.

(20) Marchese, L.; Frache, A.; Gianotti, E.; Martra, G.; Causà, M.; Coluccia, S. *Microporous. Mesoporous. Mater*. **1999**, *30*, 145.

(21) Norby, P. *J. Appl. Crystallogr*. **1997**, *30*, 21.

(22) Harding, M. M.; Kariuki, B. M. *Acta Crystallogr*. **1994**, *C50*, 852.

(23) Simmen, A.; McCusker, L. B.; Baerlocher, Ch.; Meier, W. M. *Zeolites* **1991**, *11*, 654.

(24) Oliver, S.; Kuperman, A.; Lough, A.; Ozin, G. A. *J. Mater. Chem*. **1997**, *7*, 807.

(25) Smith, L.; Cheetham, A. K.; Morris, R. E.; Marchese, L.; Thomas, J. M.; Wright, P. A.; Chen, J. *Science* **1996**, *271*, 799.

(26) Nardin, G.; Randaccio, L.; Kaucic, V.; Raijic, N. *Zeolites* **1991**, *11*, 192.

(27) Martucci, A.; Alberti, A.; Cruciani, G.; Frache, A.; Coluccia, S.; Marchese, L. *J. Phys. Chem. B* **2003**, *107*, 9655.

(28) Bennett, J. M.; Cohen, J. M.; Artioli, G.; Pluth, J. J.; Smith, J. V. *Inorg. Chem*. **1985**, *24*, 188.

(29) Pluth, J. J.; Smith, J. V. *Acta Crystallogr*. **1987**, *C43*, 866.